MNRAS 000, 1–7 (2018) Preprint 14 September 2018 Compiled using MNRAS LaTeX style file v3.0

Simulated Properties of Reionization-Epoch Galaxies: Predictions for JWST

Xiaohan Wu,[1★] Romeel Davé,[2] Jennifer Lotz,[3] Sandro Tacchella[1]
[1]*Harvard-Smithsonian Center for Astrophysics, 60 Garden St, Cambridge, MA 02138, USA*
[2]*Institute for Astronomy, University of Edinburgh, EH9 3HJ, UK*
[3]*Space Telescope Science Institute, 3700 San Martin Drive, Baltimore, MD 21218, USA*

Accepted XXX. Received YYY; in original form ZZZ

ABSTRACT
We study the photometric properties of galaxies at $z = 6$ in the Simba simulations, a suite of state-of-the-art cosmological hydrodynamical simulations. Our UV luminosity function roughly agrees with the observations, though there seems to be fewer galaxies at the bright end than observed, suggesting our simulation volume is not large enough or there may be too much dust extinction. The UV continuum slope - UV luminosity relation also roughly agrees with observations, but the bright galaxies are much bluer than in observations. This seems to suggest not enough dust extinction at the bright end, thus possibly in tension with the UV luminosity function investigations. We also generate mock images using the JWST NIRCam pixel scales and its PSFs. The size - luminosity relation obtained via these mock images is in reasonable agreement with the observations. A more interesting finding is that the sizes in rest-UV are pretty similar to that in rest-optical, though for lower mass galaxies light is more concentrated than mass. It is thus likely that these $z = 6$ galaxies are so young that the effect of a redder core in massive galaxies has not become observable yet. Our work has important implications for what can be observed by JWST, as well as constraining our understanding of galaxy formation models.

Key words: galaxies: evolution – galaxies: formation – galaxies: high-redshift – galaxies: photometry – galaxies: stellar content

1 INTRODUCTION

The Epoch of Reionization (EoR) is the era when the universe transformed from dark, cold, and neutral into hot and highly ionized, thanks to radiation from the first objects. Observing this period of the universe has always been a goal of observational cosmology, yet the EoR is just now coming within the limits of our current observational capabilities. Therefore the EoR has become one of the major scientific goals of the next generation telescopes, such as JWST. Observing the star-forming galaxies at this epoch is of particular interest, because they are thought to be the primary radiation sources that drove Hydrogen reionization.

The past decade has witnessed a number of breakthroughs in observations of these high redshift galaxies with the advent of the IR instruments on board HST. One of the most fundamental observable for galaxy studies at such high redshift is the rest-frame UV luminosity function (UVLF), which probes the volume density of galaxies over a dynamic range in luminosity. The UVLF is usually parametrized by a Schechter function(Schechter 1976), which exhibits a near power-law relation at the faint end and an exponential cutoff above a characteristic luminosity. The faint end slope of the UVLF is observed to be steeper with increasing redshift, consistent with the evolution of the halo mass function (Bouwens et al. 2015). It reaches $\simeq -2$ by $z \simeq 7-8$, suggesting that low-luminosity galaxies dominate the integrated UV luminosity during EoR. Such a steep faint end also implies that the ionizing budget produced by these early galaxies is sufficient to reionize the universe by $z \simeq 6$ (Robertson et al. 2013; Stark 2016).

While the UVLF gives the abundance of high redshift star-forming galaxies, the UV continuum slope β defined via $f_\lambda \propto \lambda^\beta$ provides information about their stellar populations and ISM. Since the UV continuum is dominated by radiation from the massive stars, the UV continuum slope of a star-forming galaxy is a function of the age and metallicity of its young populations, as well as dust extinction. At redshift $\gtrsim 6$, β is believed to be most sensitive to dust extinction, making it a useful tracer of chemical enrichment and dust formation in early galaxies (Finkelstein et al. 2012). Studies have found that galaxies are generally bluer with increasing

★ E-mail: xiaohan.wu@cfa.harvard.edu

redshift (Finkelstein et al. 2012; Bouwens et al. 2014), and that fainter galaxies bluer than brighter ones (Bouwens et al. 2015). This implies that the dust content in galaxies is decreasing towards earlier times, and that faint galaxies may be less metal enriched than massive ones.

The sizes and morphologies of galaxies in the EoR are also interesting topics of research, because galaxy size is determined by angular momentum (e.g. Mo et al. 1998) which is affected by stellar feedback (e.g. Brooks et al. 2011; Genel et al. 2015). Since the slope of the size–luminosity relation varies depending on the form of the dominating feedback (e.g. Wyithe & Loeb 2011), observing this trend gives us insights into the early evolution of these high redshift galaxies. In observations, in addition to the size–luminosity relation, galaxies at $z \gtrapprox 6$ are also found to be very compact, and sometimes contain multiple cores (e.g. Oesch et al. 2010), which could possibly be caused by mergers or several distinct star-forming regions.

Modern galaxy formation simulations offer a comprehensive cosmologically-situated framework within which to understand and interpret such EoR observations. For instance, the simulations of Davé et al. (2006) are shown to generate UV and Lyα LFs that are in reasonable agreement with observations at $z \sim 6-9$, and a stellar feedback model with momentum-driven winds is mildly favored. Finlator et al. (2011) demonstrated that the smoothly rising star formation histories of simulated galaxies at EoR can account for the observed UVLFs and stellar mass densities at $z = 6-8$. More recent simulations like Finlator et al. (2018) have included radiative transfer, and are used for not only studying the galaxy properties, but also the intergalactic medium and the circumgalactic medium. These works have set a solid foundation for making comparisons between simulations and observations, as well as making predictions for upcoming observations.

In this work, we use galaxies at $z \sim 6$ from the Simba simulations, the successor to the Mufasa project (Davé et al. 2016), to study how their photometric properties compare with observations. The simulations are mildly calibrated using observational data at low redshift, so this comparison aims to test this model at high redshifts, in addition to providing physical insights into the nature of EoR galaxies. Additionally, such state-of-the-art simulations provide a powerful platform to make predictions for upcoming observational facilities such as JWST. Compared to HST, JWST allows us to probe the rest-frame optical radiation from those $z \sim 6$ galaxies. Thus making predictions for both the rest-UV and rest-optical observations and linking them will be particularly interesting when looking into the properties of simulated galaxies.

This paper is organized as follows. In Section 2 we briefly introduce the simulations and the tools we use to generate mock observations. In Section 3 we present the main results: the UVLF, UV continuum slope, and size measurements from the simulated galaxies. In Section 4 we discuss possible future directions and summarize our work.

2 METHODS AND SIMULATIONS

We extract galaxies at $z = 6$ from two sets of Simba simulations, one with a box size of 25 Mpc/h, the other 12.5 Mpc/h. Both runs use 512^3 gas fluid elements and 512^3 dark matter particles, giving a dark matter particle mass of 1.2×10^7 M$_\odot$ and 1.5×10^6 M$_\odot$ respectively. The minimum gravitational softening lengths are 0.25 kpc/h and 0.125 kpc/h respectively for these two simulations. We will denote them by m25n512 and m12.5n512 for the rest of the paper. Galaxies are identified using a minimum star particle number requirement of 32. This gives us 274 galaxies in m12.5n512 and 514 galaxies in m25n512.

In order to mock observations and obtain the photometric properties of the simulated galaxies, we use the Pyloser package [1]. Pyloser treats each simulated star particle in a galaxy as a single stellar population formed at the time the star particle was created, with a given metallicity, and generates a mock spectrum using the Flexible Stellar Population Synthesis (FSPS) library of population synthesis models (Conroy et al. 2009; Conroy & Gunn 2010) including nebular emission. Dust extinction is obtained by calculating an A_V value for each star particle, based on the integrated metal column density along the line of sight to it. For default we assume an extinction curve of the Salmon et al. (2016) form, but we have also tried using the Calzetti et al. (2000) extinction law. The Salmon et al. (2016) extinction law is a modification to the Calzetti et al. (2000) law. It multiplies the Calzetti et al. (2000) law by $(\lambda/\lambda_V)^\delta$, where $\delta = 0.62 \log E(B-V) + 0.26$ and λ_V is the $V-$band wavelength of 5500 Å. Such a form lets galaxies with high color excess have a shallower, starburst-like law, and those with low color excess have a steeper, SMC-like law. Pyloser convolves the summed spectra within a given galaxy or pixel with different filters, in order to obtain magnitudes in different bands. This is done using both the rest-frame spectra and the redshifted spectra, in order to calculate the UVLF and the UV continuum slope and get observed-frame fluxes in JWST bands respectively. We especially focus on JWST F115W and F444W, which correspond to rest-frame 1600 Å and 6200 Å at $z = 6$.

In Fig. 1 we show an example of mock spectra generated for a galaxy in the m12.5n512 simulation. This galaxy has a stellar mass of 5.4×10^8 M$_\odot$ and a SFR of 1.2 M$_\odot$/yr. Its A_V value is 0.16. It can be seen that the Calzetti et al. (2000) extinction law generates a bit more dust extinction at shorter wavelengths, compared to the Salmon et al. (2016) law.

3 MAIN RESULTS

In this section we present our measurements of the UVLF, UV continuum slope, and galaxy sizes.

3.1 UVLF

In Fig. 2 we show the simulated rest-frame 1500 Å LFs at $z = 6$ compared with the observational data from Bouwens et al. (2015). Here we use all galaxies in our sample. Since these small young objects are very gas-rich, they typically have $\gtrsim 100$ gas and star particles in total, which is generally regarded as sufficient to be well-resolved.

[1] https://pyloser.readthedocs.io/en/latest/

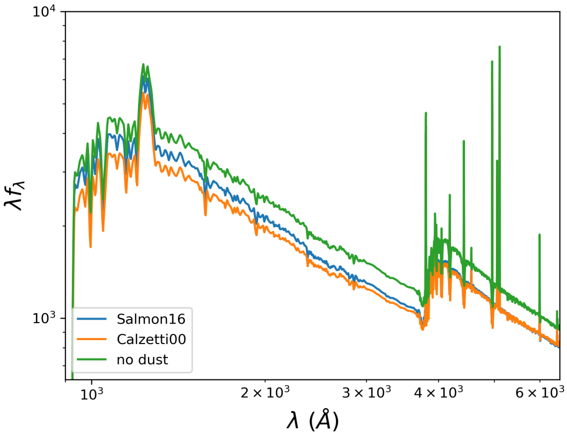

Figure 1. Mock spectra of a galaxy having $A_V = 0.16$. Cases of assuming a Salmon et al. (2016) extinction law (blue), a Calzetti et al. (2000) extinction law (orange), and no dust (green) are shown.

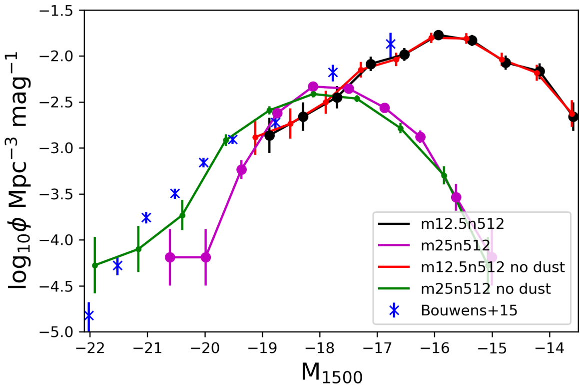

Figure 2. The UVLFs obtained from the m25n512 and m12.5n512 simulations, assuming a Salmon et al. (2016) extinction law. Also shown are the UVLFs without dust extinction. The observational data points are shown in blue, which come from Bouwens et al. (2015).

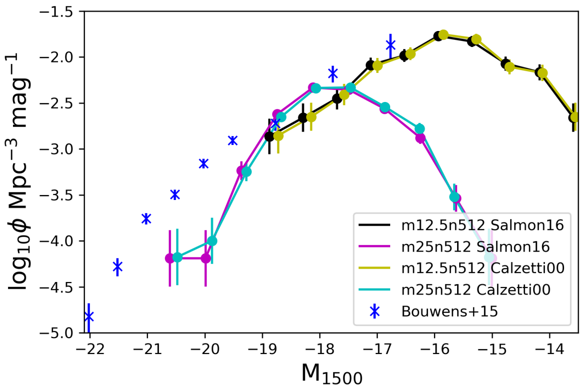

Figure 3. A comparison among the UVLFs obtained by assuming the Salmon et al. (2016) extinction law, the Calzetti et al. (2000), and no dust.

It can be seen that in the M_{1500} range of $[-19, -16]$, the simulated UVLF roughly agree with observations, so the galaxy formation model adopted by Simba is broadly successful in reproducing the observed abundances of $z = 6$ galaxies. The turn-over fainter than $M_{1500} \approx -16$ is a numerical resolution effect. At the bright end, however, the simulations seem to produce too few galaxies compared with observations. One possible reason is that we may be adding too much dust extinction, which especially affect the bright galaxies. We also noticed during our computation of the dust extinction that at a fixed M_{1500}, galaxies in the m25n512 simulation have larger A_V values than those in the m12.5n512 run, so numerical convergence may also be responsible for the simulated UVLF being lower than observed at the bright end. However, as shown in Fig. 2, the m25n512 UVLF without dust only marginally match the observational data, while we would naively assume it to be higher than the observed points. This means a simulation with a larger volume would be more helpful in bringing the simulated UVLF to agreement with observations. Therefore in future work, we will include analysis from a 50 Mpc/h run, as well as simulations of even higher resolution.

For completeness, we show in Fig. 3 the UVLFs obtained by assuming a Calzetti et al. (2000) extinction law. The Calzetti et al. (2000) law would generate more extinction than Salmon et al. (2016) law as shown in Fig. 1, but the UVLFs do not change much when we change the extinction curve. So our results are relatively robust with the assumption of extinction laws, for galaxies fainter than -21 mag.

3.2 The UV Continuum Slope

We next consider the simulated β - M_{1500} relation, as shown in Fig. 4. This again assumes a Salmon et al. (2016) extinction law. For obtaining this curve, we adopt a more conservative 128 star particle number cut in order to make sure there are enough number of star particles to sample the galaxy star formation history particularly at small ages that dominate the M_{1500} flux. This criterion leaves us 59 galaxies in m12.5n512 and 91 galaxies in m25n512. β is obtained by fitting the fluxes at 1500 Å, 2300 Å, and 2800 Å using $f_\lambda \propto \lambda^\beta$. The no dust case essentially flattens the β - M_{1500} relation, suggesting the importance of β as a tracer of dust attenuation, which is especially important for bright galaxies as they suffer more from dust extinction. Our simulated β roughly agree with the Bouwens et al. (2014) observations within the error-bars, for galaxies fainter than about -19 mag, though the simulated galaxies may be a bit bluer than observed. At the bright end, however, the discrepancy becomes clearer, implying that our simulated galaxies are too blue. A natural explanation is that the bright galaxies are not extincted enough, so we are possibly not producing enough metals.

If use the Calzetti et al. (2000) extinction law, the β - M_{1500} relation can be brought into better agreement with observations, as shown in Fig. 5. The bright galaxies are obviously redder under the assumption of the Calzetti et al.

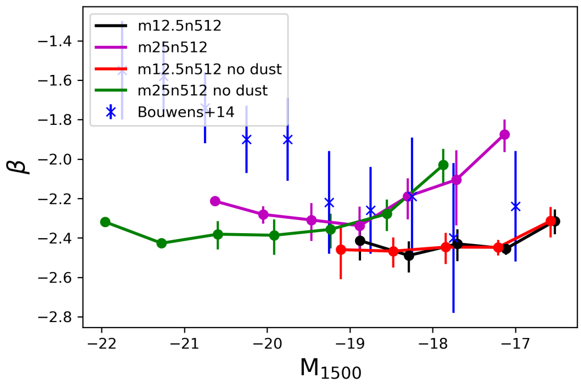

Figure 4. The β - M_{UV} relations obtained from the m25n512 and m12.5n512 simulations, assuming a Salmon et al. (2016) extinction law as well as no dust extinction. The observational data is from Bouwens et al. (2014).

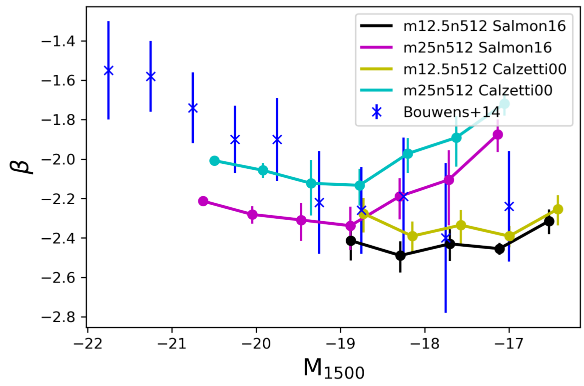

Figure 5. A comparison among the β - M_{UV} relations obtained by assuming the Salmon et al. (2016) extinction law, the Calzetti et al. (2000), and no dust.

(2000) extinction curve, though still a bit bluer than observed galaxies at $M_{1500} = -21 \sim -20$. Therefore the form of the extinction law does not fully resolve the tension between our simulations and observations, but it is likely that the Calzetti et al. (2000) law is more suitable to describe the dust extinction in high redshift galaxies than the Salmon et al. (2016) law. It will also be useful to include galaxies from the 50 Mpc/h box run to see the behavior of galaxies even brighter than -21 mag, though we must bear in mind that the A_V values are not fully converged. But all in all, the simulations are in reasonable agreement with observations.

We notice that the simulated β - M_{1500} relation for galaxies fainter than ~ -19 mag seem to flatten. Although Bouwens et al. (2014) also found a slightly shallower slope for the β - M_{1500} relation at the faint end, the flattened curve generated by the simulations is likely a numerical artifact. Fainter galaxies do not have high enough numbers of star particles to fully sample their star formation histories. Increasing the mass resolution by a factor of 8 brings the value of β down, as can be seen in the $M_{1500} = -19 \sim -17$ range. Similarly, the upturn of the β - M_{1500} relation for the m25n512 dataset is also a numerical effect. Simulations with higher resolution will help improve these curves, but conclusions drawn from the curves should be taken with a grain of salt.

3.3 Galaxy Size and Morphology

In this section we present a measurement of galaxy sizes and the comparison to observations. In particular we focus on sizes in the JWST F115W band and in JWST F444W band. We generate mock JWST images and do the size measurements via three methods:

- In method 1, we generate both the F115W images and the F444W images using the F115W pixel scale, 0.031 arcsec. F444W images created in this way are denoted by high resolution (HR). A segmentation map is created for the F444W image and we measure a flux weighted center based on the segmentation map. The half light radius is defined as the radius containing half of the total light of the galaxy, obtained by calculating the curve of growth. We use the same segmentation map and image center for measuring the half light radius of the F115W image.
- In method 2, the F444W images are generated using the F444W pixel scale, 0.063 arcsec, called low resolution (LR) in our case. Size measurements are done in the same way as in method 1, and we still use the F444W segmentation maps and image centers to measure the F115W sizes.
- In method 3, we convolve the F115W and LR F444W images with the corresponding PSFs and add Gaussian noise to it. We achieve a signal-to-noise ratio of roughly 10 for the bright galaxies. The sizes are then obtained by obtaining segmentation maps and doing Sersic fit, using the statmorph code (Rodriguez-Gomez et al. (in prep.)). The statmorph code returns flags for the Sersic fit. We distinguish galaxies with good fitting flags and those with bad fitting flags.

An illustration of the three methods are shown in Fig. 7. We also show an example of mock images in Fig. 6, in both HST bands and JWST bands, though the images are not convolved with PSF and no noise is added. For mock image generation we assume a Salmon et al. (2016) extinction law. We have not explored a different extinction curve yet.

The resulting F115W size - luminosity relations using the three methods for m25n512 and m12.5n512 galaxies are shown in Fig. 8. Again we use galaxies with larger than 128 star particles. And for method 3, we only include galaxies with good Sersic fits in this figure. First it is noticeable that the sizes are not converged with this resolution, so the m25n512 results should be taken with a grain of salt. The m12.5n512 results roughly agree with the observations, although the sizes of simulated galaxies are a bit larger than observed. The size - luminosity curve for the m25n512 galaxies seem to exhibit an upturn at the bright end. It is hard to say whether such an upturn is caused by the sizes being not converged at magnitudes lower than -19, but we notice that the brightest galaxies in Bowler et al. (2017) are significantly larger than fainter ones because they contain multiple components, although such galaxies in their samples are brighter than -21 mag. A visual check of our bright galaxies indicates that they are indeed clumpy, but the simulated galaxies seem to contain many more smaller clumps

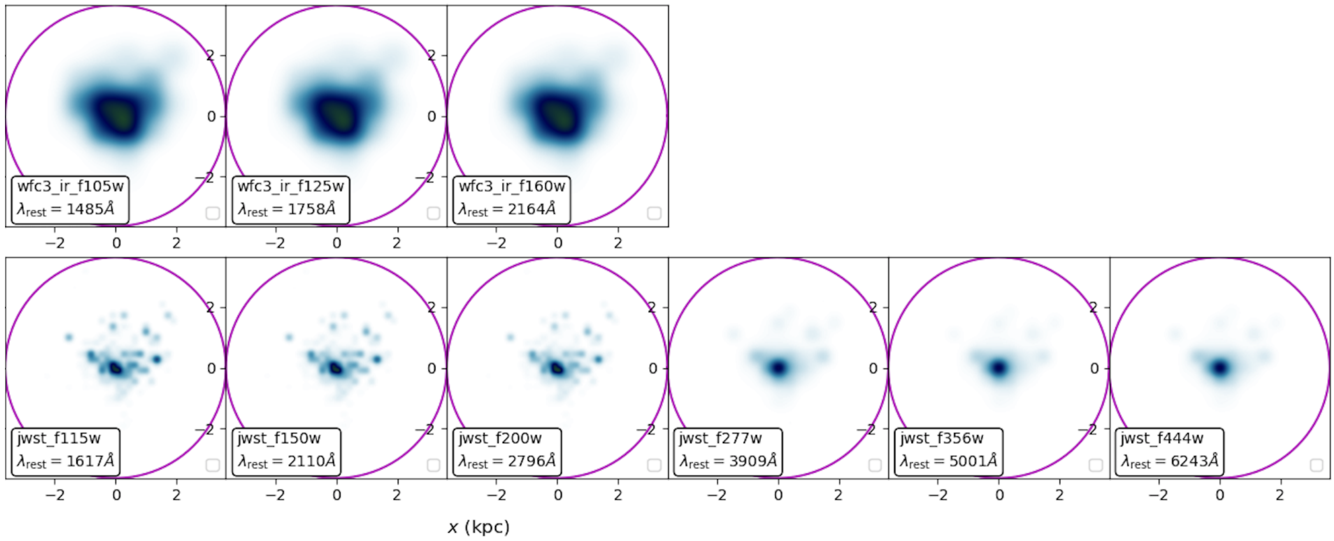

Figure 6. An example of mock images of a galaxy in m12.5n512. Shown are mock images in three HST IR bands and six JWST bands. The images have not been convolved with PSFs and no noise has been added.

than the ones shown in Bowler et al. (2017), for instance like the one shown in Fig. 6. A comparison with the 50 Mpc/h run will be helpful since it contains even brighter galaxies. It will be seen whether such an upturn still exists for brighter galaxies.

In Fig. 9 we compare the sizes in F115W band with the sizes in F444W band. What is most interesting is the sizes measured using method 1, since method 2 and 3 exhibit instrumental effects. We find that the simulated galaxies at $z = 6$ have very similar sizes in the rest-frame optical (F444W) and the rest-frame UV (F115W), which is surprising because this is not expected for galaxies at much lower redshifts where the cores are redder and the disks are bluer. Our size measurements at $z = 6$ implies that these much higher redshift galaxies are so young that even if they possess a redder core, the effects on the sizes are not evident yet. This would be an interesting aspect for JWST to probe.

We also compare how the half light radius recover the stellar half mass radius. The stellar half mass radius is measured using the curve of growth of the F444W image and its segmentation map. The fractional difference between the half light radius and the stellar half mass radius is shown in Fig. 10. Although the scatter is large, there is a clear trend that for less massive galaxies, light is more concentrated than mass, which is consistent with a central starburst scenario. For higher mass galaxies, the half light radius is comparable to or even larger than the stellar half mass radius. It is possible that these galaxies have begun to exhibit features of a redder core, but based on Fig. 9, the effects may not be so prominent yet. In principal, we could separate the contributions of light from younger and older populations to investigate this further.

4 DISCUSSIONS AND CONCLUSIONS

In this work, we studied the photometric properties of galaxies from the Simba m25n512 and m12.5n512 simulations. We find reasonable agreement of the simulate UVLF, β - M_{1500} relation, and size - luminosity relation with observations. Tensions also exist, for instance the brightest galaxies do not seem to be dust attenuated enough, possibly implying that metals are not produced enough in the simulations at such high redshift. The simulated galaxies also seem to have a bit larger sizes than observed galaxies, especially for the brighter ones. However the observational uncertainties are large as well. Future observational facilities such as JWST will be able to yield more accurate measurements and give more hints on our understanding of the galaxy formation models.

In the near future, we will apply the same measurements to the Simba m12.5n1024, m25n1024, and m50n1024 simulations, which have even higher resolution and will also allow us to probe a larger dynamic range in galaxy luminosity. It will be useful to try different extinction laws as well and determine which ones better fit observations. An extension to other redshifts can be another good future step to go, since we can explore the redshift dependence of these photometric properties as found in observations. It will also be interesting to compare with other simulations of similar resolutions, especially IllustrisTNG50, to see how different implementations of feedback affects the statistics. We can also apply the JWST GTO source selection criteria to our simulated galaxies and make direct predictions for what JWST would expect to observe. Besides these, there are also other quantities of the simulated galaxies that we can look into, such as their concentration, dust extinction distribution etc. These will let us understand the physical properties of high redshift galaxies better.

ACKNOWLEDGEMENTS

We would like to thank the support of the Kavli summer program in astrophysics, the sponsorship of the Kavli Foundation, the National Science Foundation, and UC Santa Cruz.

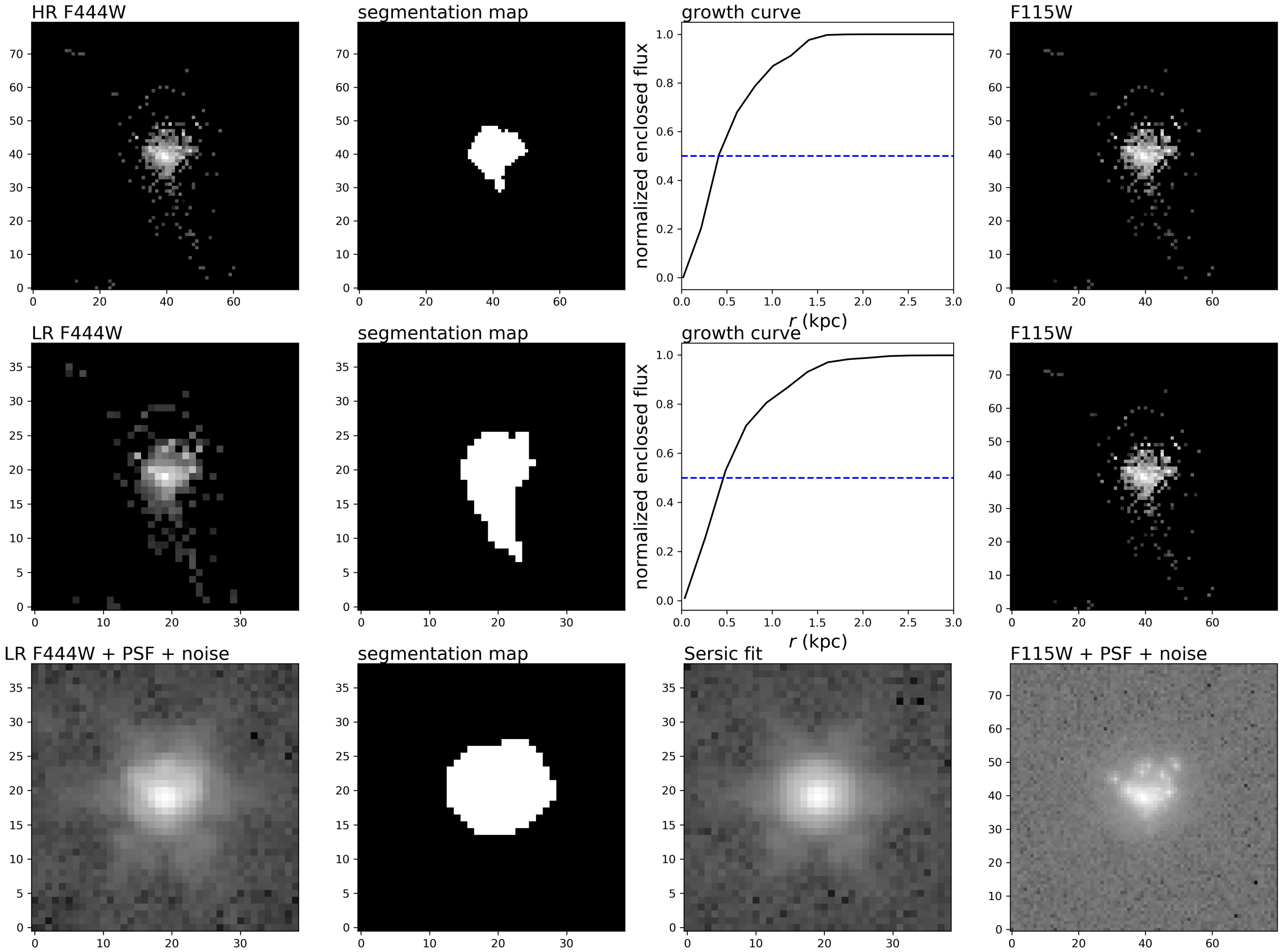

Figure 7. An example of how we measure galaxy sizes. The upper, middle, and lower panels represent method 1, 2, 3 respectively. The first three panels in the upper row are the high resolution JWST F444W image, the corresponding segmentation map, and the curve of growth. The middle panel consist of the same figures except that the F444W image is now of low resolution. The rightmost panel shows the F115W image, which is always generated at the F115W pixel scale. The lower panel illustrate the F444W image after convolving with PSF and adding noise, its corresponding segmentation map, the Sersic fit to the image, and the F115W image after convolving with PSF and adding noise.

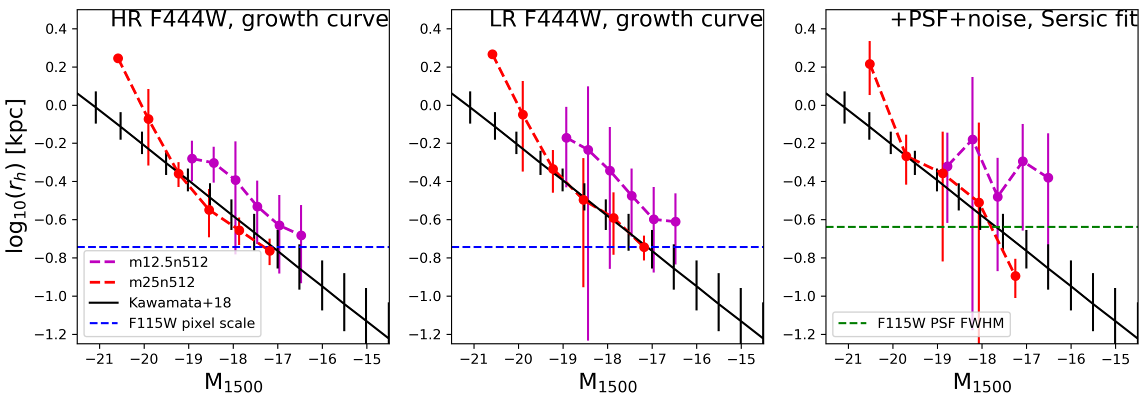

Figure 8. Size - luminosity relation for the m25n512 and m12.5n512 galaxies. Sizes refer to that measured in F115W mock images. The blue dashed line shows the pixel size of the F115W filter, and green dashed line indicates the FWHM of the F115W PSF. The black line with error-bars show the observational result from Kawamata et al. (2018). Panels from left to right represent size measurements using method 1, 2, 3 respectively.

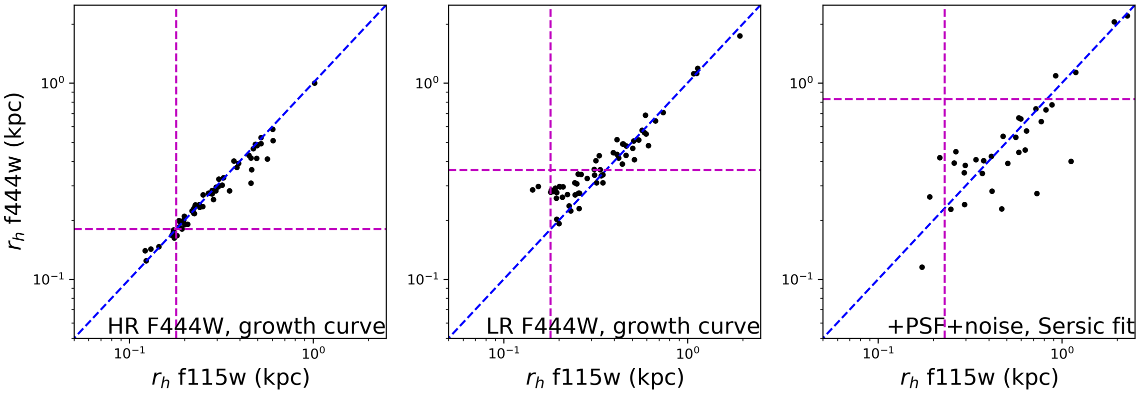

Figure 9. Comparison between sizes measured in F444W and that measured in F115W. From left to right size measurements are done using method 1, 2, 3 respectively. The magenta dashed lines in the right panel show the pixel scale of the F115W filter and the F444W filter.

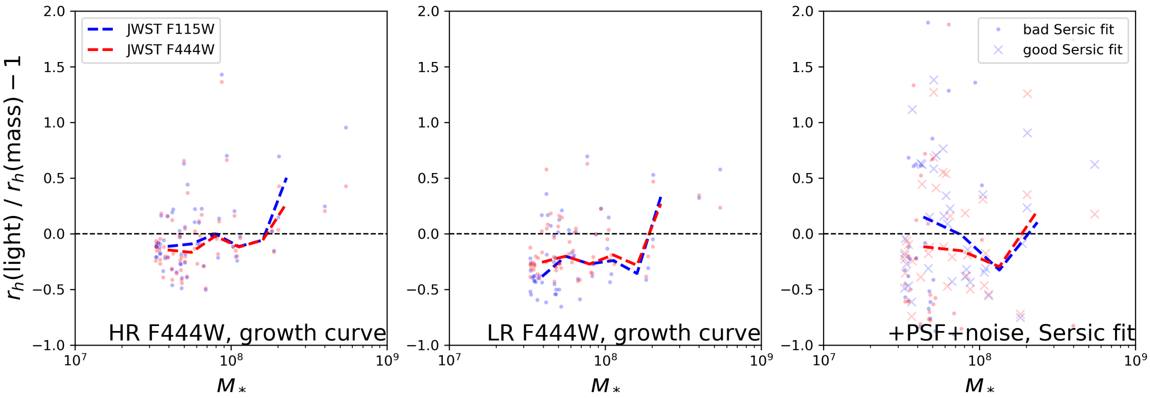

Figure 10. The fractional deviation of the half light radius from the half stellar mass radius as a function of stellar mass. From left to right sizes are measured using method 1, 2, 3 respectively. For method 3, good and bad fits are determined by the flags returned by the statmorph code.

REFERENCES

Bouwens, R. J., Illingworth, G. D., Oesch, P. A., et al. 2014, ApJ, 793, 115
Bouwens, R. J., Illingworth, G. D., Oesch, P. A., et al. 2015, ApJ, 803, 34
Bowler, R. A. A., Dunlop, J. S., McLure, R. J., & McLeod, D. J. 2017, MNRAS, 466, 3612
Brooks, A. M., Solomon, A. R., Governato, F., et al. 2011, ApJ, 728, 51
Calzetti, D., Armus, L., Bohlin, R. C., et al. 2000, ApJ, 533, 682
Conroy, C., Gunn, J. E., & White, M. 2009, ApJ, 699, 486
Conroy, C., & Gunn, J. E. 2010, ApJ, 712, 833
Davé, R., Finlator, K., & Oppenheimer, B. D. 2006, MNRAS, 370, 273
Davé, R., Thompson, R., & Hopkins, P. F. 2016, MNRAS, 462, 3265
Finkelstein, S. L., Papovich, C., Salmon, B., et al. 2012, ApJ, 756, 164
Finlator, K., Oppenheimer, B. D., & Davé, R. 2011, MNRAS, 410, 1703
Finlator, K., Keating, L., Oppenheimer, B. D., Davé, R., & Zackrisson, E. 2018, MNRAS, 480, 2628
Genel, S., Fall, S. M., Hernquist, L., et al. 2015, ApJ, 804, L40
Kawamata, R., Ishigaki, M., Shimasaku, K., et al. 2018, ApJ, 855, 4
Mo, H. J., Mao, S., & White, S. D. M. 1998, MNRAS, 295, 319
Oesch, P. A., Bouwens, R. J., Carollo, C. M., et al. 2010, ApJ, 709, L21
Robertson, B. E., Furlanetto, S. R., Schneider, E., et al. 2013, ApJ, 768, 71
Salmon, B., Papovich, C., Long, J., et al. 2016, ApJ, 827, 20
Schechter, P. 1976, ApJ, 203, 297
Stark, D. P. 2016, ARA&A, 54, 761
Wyithe, J. S. B., & Loeb, A. 2011, MNRAS, 413, L38

This paper has been typeset from a TEX/LATEX file prepared by the author.